# Supramolecular Coordination Polymer Nanotube Additive for Enhanced Performance and Reduced Emission in Diesel Engines Using Biodiesel/Diesel Blend Fuels

Mona M. Fouda<sup>1</sup>, Safaa E. H. Etaiw<sup>1</sup>, Dina M. Abd El-Aziz<sup>1</sup>, Medhat Elkelawy<sup>2,3</sup>, Hagar A. Bastawissi<sup>3</sup>

<sup>1</sup>Chemistry Department, Faculty of Science, Tanta University, Tanta, Egypt

E-mail: dina.abdelaziz@science.tanta.edu.eg

**Abstract**. Single-crystal and powder X-ray diffraction, electron microscopy (TEM and SEM), and elemental analysis were used to characterize the nano-tube supramolecular coordination polymer { $[Cu_6(CN)_6] \cdot HDA}n$ , (**NTSCP**); (HDA=heptan-1,7-diamine). Both copper atoms have a tetrahedral shape and are coordinated with cyanide ligands. Cu1 and Cu2 create the unique cluster structure of two quadruple  $[Cu_2(\mu^3 - CN)_2]$  units exhibiting coprophilic interaction. The development of channels of dimensions 8.917-15.270 nm that stretch three-dimensionally to create fused nanotubes with various shapes is indicated by the structure of **NTSCP**. In this paper, the prepared nano-tube SCP has been used as a chemical and physical properties enhancer to the west cooking oil biodiesel/diesel blended fuel in direct injection diesel engines. Fuel efficiency can be significantly increased by using NTSCPs, which are effective additives that enhance combustion characteristics and reduce emissions. The engine brake thermal efficiency, exhaust gas temperature, and flue gas concentrations were tested at different engine loads and fixed speeds of 1500 RPM. The experimental data of the engine indicate a consistent and promising engine performance, along with favourable emissions positive results.

**Keywords:** Nanotube supramolecular coordination polymer (NTSCP); Engine emissions; Biodiesel/Diesel blend; Engine performance and emissions; Multifunctional nanoparticles additives

## 1. Introduction

Biomass energy generation presents a viable pathway to reduce dependency on fossil fuels while addressing environmental concerns. Biomass, originating from organic materials like agricultural and wood waste, may be transformed into biofuels, biogas, and bio-natural gas. So, it can substantially reduce emissions of greenhouse gases and improve energy safety [1]. In 2017, the United Nations adopted Sustainable Development Goal 7 (SDG7). SDG7 aims to guarantee universal access to cheap, dependable, and renewable energy services by 2030. This requires extending access to clean fuels, and technology, as well as improved energy efficiency and boosted use of renewable energy [2]. Following

<sup>&</sup>lt;sup>2</sup>Mechanical engineering department, Faculty of Engineering, Pharos University in Alexandria, Alexandria, Egypt

<sup>&</sup>lt;sup>3</sup>Mechanical Power Engineering Department, Faculty of Engineering, Tanta University, Tanta, Egypt

SDG7, conversion methods which include thermal, chemical, and biological processes, enable efficient energy generation from biomass waste. This conversion will make it a less expensive alternative to fossil fuels [3]. Besides, the biomass integrated into hybrid energy systems may enhance the generation of energy while minimizing environmental consequences. Biomass is sustainable and contributes to gaining a low-carbon economy [4].

Research shows that switching to biodiesel from fossil fuels significantly lowers CO<sub>2</sub> emissions. Biodiesel is a desirable alternative for communities that are seeking to become energy-independent because it can be produced using a variety of feedstock. The physicochemical properties of biodiesel enhance its applicability in existing engines when compared to those of conventional diesel [5,6].

Nanoparticles such as, (titanium dioxide (TiO<sub>2</sub>), aluminum oxide (Al<sub>2</sub>O<sub>3</sub>), Nano-supramolecular coordination polymers (NSCP)...etc), have demonstrated a great deal of promise in improving internal combustion (IC) engine emissions and fuel economy, particularly when used as additives in biodiesel blends [7]. The chemical, physical, and biological characteristics of materials at the nanoscale are distinct from those of their bulk counterparts. These characteristics originate from their increased surface area to volume ratio, quantum effects, and superior reactivity [8]. Arabs are often recognized as early pioneers of nanotechnology through their development of Damascus steel [9]. The calorific value and cetane number of fuels are improved by the inclusion of nanoparticles. Accordingly, uncompleted combustion product emissions decline, and combustion properties are enhanced [7]. Overall, using nanoparticles strategically can improve engine performance and help create cleaner combustion processes, which will solve issues with efficiency and the environment [10].

NSCPs are efficient additives that improve combustion characteristics and lower emissions, which can greatly increase fuel efficiency. Additionally, by acting as oxygen buffers, NSCPs can promote better combustion and produce up to 80% less hazardous emissions of CO and NO<sub>x</sub>. Therefore, including nanoparticles in fuel formulations offers a viable way to enhance IC engines' performance and environmental effects [11]. So, in this work, the use of Nanotube supramolecular coordination polymers (NTSCP) additives in diesel/biodiesel blended fuel as enhancers of physical and chemical properties has been experimentally investigated. The fuel blends were used to power a direct-injection diesel engine. The tested engine is water-cooled and naturally aspirated, operating under varying loads and a fixed speed of 1500 RPM. Thermal efficiency of the engine brake, along with the exhaust gas temperature and flue gas concentration, was meticulously recorded at different NTSCP additives concentrations.

#### 2. Experimental

#### 2.1 Materials and physical measurements

Chemicals and solvents of analytical quality were used.  $K_3[Cu(CN)_4]$  was synthesized according to the methodology outlined in the literature [12]. The instrumentation used in the investigation was the same as previously stated [12]. Measurement of XRD single crystal data of **NTSCP** had been performed using a Kappa CCD Enraf Nonius FR 90 four circle-goniometer with graphite monochromatic MoK $\alpha$  radiation {[ $\lambda$ MoK $\alpha$ ] = 0.71073Å. Structure refinement parameters and crystal data of **NTSCP** were completely discussed and articulated by earlier authors' research [12].

## 2.2 The procedure of synthesising NTSCP $\infty^3$ [(Cu<sub>3</sub> (CN)<sub>3</sub>)<sub>2</sub> (DAHP)]

 $K_3[Cu(CN)_4]$  [178 mg (0.63 mmol)], Me<sub>3</sub>SnCl [380 mg (1.9 mmol)] and heptane-1,7-diamine (HDA) [82 mg (0.63 mmol)] have been reacted in H<sub>2</sub>O/acetonitrile solution under ultrasonic waves for four h (using a power of 70 W at 30 °C). Colorless needle crystals (**NTSCP**) were produced after a month. The product was filtered off, washed with acetonitrile/ H<sub>2</sub>O then dried under vacuum. 257 mg (60%) of **NTSCP** was attained. Anal. Calcd. for **NTSCP** (C<sub>13</sub> H<sub>18</sub> N<sub>8</sub> Cu<sub>6</sub>) M.W. = 667.61 g mol –1: C, 23.39; H, 2.72; N, 16.78.; Cu, 57.11, Found: C, 23.43; H, 2.64; N, 16.59; Cu. 57.08%.

## 2.3 Fuel blend preparation with NTSCP additive

NTSCP was dissolved in methanol to create 100 and 200 ppm concentrations. The pH of the produced nanofluids was adjusted to 10 using 0.1 M NaOH. Diesel/biodiesel blend (B60) was prepared by mixing biodiesel with diesel fuel at a ratio of 60:40 V/V%, respectively. The B60 blend has been placed inside a glass beaker and agitated with a mixer for two continuous hours to achieve proper mixing. NTSCP Nanofluids were mixed with B60 blends and then subjected to ultrasonic radiation for one hour. The effect of various concentrations of NTSCP Nanofluids on the engine's emissions and efficiency was then examined.

## 2.4 Engine test rig methodology

Single-cylinder diesel engines are an important aspect of vehicle engineering and environmental sustainability. It is critical to evaluate the performance and emissions of single-cylinder diesel engines fed with various fuel additives. The hydraulic dynamometer technique is used to assess engine performance and emissions under different load circumstances, from no load to maximum engine capacity, at a constant speed. Incremental loads at a constant speed were used to imitate real-world operating circumstances and evaluate the response of the engine in terms of power production, emissions, and fuel consumption. Tests were performed using a single-cylinder, 4-stroke compression ignition engine "S1100A2". A hydraulic dynamometer "ATE-160 LC" was used to measure engine power. Exhaust gases emitted during various tests such as CO, CO<sub>2</sub>, UHCs, O<sub>2</sub>, and NO<sub>x</sub> were measured quantitatively using an "HPC500/400" automotive emissions analyzer. The engine's rotational speed has been set at 1500 rpm. The schematic diagram of the engine setup, along with an actual photograph of its configuration with different measuring arrangements were completely discussed and presented by the previous authors' work [11]. Data for all engine parameters have been calculated. The total error of the measured data has been equated (1) as follows:

$$W_{R} = \left( \left( \frac{\partial R}{\partial x_{1}} W_{1} \right)^{2} + \left( \frac{\partial R}{\partial x_{2}} W_{2} \right)^{2} + \dots + \left( \frac{\partial R}{\partial x_{n}} W_{n} \right)^{2} \right)^{\frac{1}{2}}$$
(1)

 $W_R$  represents the total error for the measured value.  $W_1, W_2, ..., W_n$  symbolizing the errors of individual parameters. The error values for emissions parameters fell within the range of  $\pm 0.25\%$ . The values  $\pm 0.15\%$ ,  $\pm 1.1\%$ , and  $\pm 0.65\%$  represent the errors of the K-type thermocouple, air flow rate, and fuel flow rate, respectively.

## 3. Results and Discussion

# 3.1 Characterization of the NTSCP

By adding the complex  $K_3[Cu(CN)_4]$  and  $Me_3SnCl$  to HDA under ultrasonic waves, the tin-free  $\{[Cu_6(CN)_6]\cdot DAHP\}n$  (NTSCP) was created. The main building unit  $[Cu\ CN]_3$  and a half unit of free HDA, figure S1, make up the asymmetric unit. While the copper atoms have different crystal structures, they are coupled to form tetrahedral-shaped C-N ligands. The attractive cluster growing up of the couple  $[Cu_2(\mu^3-CN)_2]$  rhombic pieces attached by Cu2 is created by Cu1 and Cu2 figures 1 and S1. The quadruple fragment, table S1, is formed by the acquisition of two linear C-N ligands (173.15-176.28°) and two bent C-N ligands (125.38-153.45°) by the Cu1 geometry.

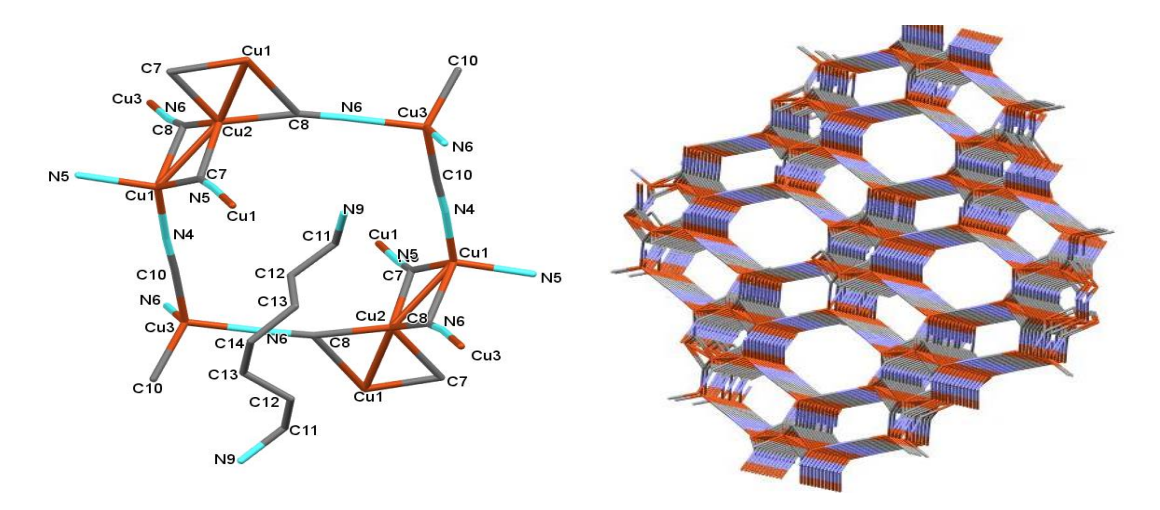


**Figure 1.** Ortib representation of **NTSCP** in the **Figure 2.** Vision of the 3D-nanotube ac-plane indicating the coordination topology of the copper atoms, the guest 1,7-DAHP, two joined couples of the bifurcated [Cu<sub>2</sub>(µ<sup>3</sup>CN)<sub>2</sub>] motifs and the [Cu<sub>6</sub>(CN)<sub>6</sub>] ring structure. Hatoms are removed for clarity.

structure of NTSCP along the c-axis.

Conversely, the cluster segments displaying coprophilic contact (2.52 nm) are connected by four bent C≡N ligands (132.98-165.76°) that are coordinated to the Cu2 site. Figure 1 shows the dihedral angle of the two rings (89.56°). Four linear C-N ligands (173.47-177.76°) are present in the tetrahedral geometry of Cu<sub>3</sub>, as seen in table S1. To enclose the guest long chain DAHP (8.22Å), the [Cu<sub>3</sub>(CN)<sub>3</sub>] units are the building blocks of NTSCP that are organized in a special, attractive topology. The bent structure acquired by the guest HDA has an angle C13-C14-C13 = 116.98°. To accommodate the guest HDA, [Cu<sub>3</sub>(CN)<sub>3</sub>] units in this instance form fused deformed rectangular rings encircled by rhombic motifs displaying expanding voids figure S3. It is commonly known that the C-N ligand connects two metals in a linear form, however, it is quite uncommon for the carbon atom to coordinate two metals as is typical in the carbonyl moiety. The [Cu<sub>2</sub>(CN)<sub>2</sub>] units, which currently serve as the primary building blocks of an increasing number of multidimensional supramolecular collections, exhibit aberrant cyanide bridging behaviour. Although it is commonly recognized that the CuI atom often attaches to the cyanide group through its carbon end, [Cu<sub>2</sub>(CN)<sub>2</sub>] motifs with direct carbon or nitrogen bridges are currently unable to be detected. There are µ4-CN units in the polymer of [(CuCN)<sub>2</sub>-piperazine] where the nitrogen and carbon atoms coordinate to form two copper atoms [13,14].

For instance, NTSCP, two copper atoms are joined by the carbon end of the CN ligand. For tiny nonmetals, distinct coordination numbers were produced among the gold (I) complexes. In the special instance [C(AuPR<sub>3</sub>)<sub>6</sub>] apart from six coordination, a carbon atom is present in the 2+ cation. Even though the carbon atom is believed to lack low energy d-orbitals, a1g (2S) and t1u (2P) can be created to form three centre bonds which is like the bonding in diborane [14].

The word "coprophilicity" was used to represent the Cu1–Cu2 bonding interaction. That the shorter Cu....Cu distances; e.g., Cu(1)...Cu(2) = 2.51 Å, table S1, in the  $[Cu_2(\mu^3-CN)_2]$  rhombs, are attributable to effective cyanide bridging. Interestingly, compared to metallic copper (2.55 Å), the Cu....Cu connections are only somewhat shorter. In addition, a close examination of the structure of NTSCP shows that nanotubes with diameters of 8.917-15.270 nm have been formed figure S2. As seen in figures 2, and S2, the structure of NTSCP grows to 3D, producing fused tubes with a variety of shapes. The network of **NTSCP** is further stabilized by the guest HDA through H-bonds ((2.36-2.79 Å), table S2. The characteristic absorption band in **NTSCP**'s infrared spectrum is represented by the  $v_{CN}$  band. The  $v_{CN}$  supports nonlinear bridging of [(Cu<sub>3</sub> (CN)<sub>3</sub>)<sub>2</sub>] system, resulting in two strong bands at 2110 and 2091 cm<sup>-1</sup>. The presence of amino groups in H-bonds is shown by the appearance of their  $v_{NH}$ ,  $\delta_{NH}$ , and  $\gamma_{NH}$  bands at 3208 and 3230 cm<sup>-1</sup>, 1579-1583 cm<sup>-1</sup>, and 700-713 cm<sup>-1</sup>. The  $\gamma_{CH}$  band is seen around 776-864 cm<sup>-1</sup>, while the CH<sub>2</sub> groups of DAHP absorb at 2921 and 2860 cm<sup>-1</sup> due to  $v_{CH}$  and at 1469 cm<sup>-1</sup> due to  $\delta_{CH}$ . The  $v_{Cu-C}$  bond is located at 484 cm<sup>-1</sup> as a faint band. TEM images support the presence of regular nanostructures and narrower morphology with particle size 2.20-33.66 nm and cavity size 45.62-79.13 nm, figure 3(a and b). SEM was designed for directly studying the surfaces of solid objects which support the regular nano structure of **NTSCP** appearing like rods, figure 3(c and d).

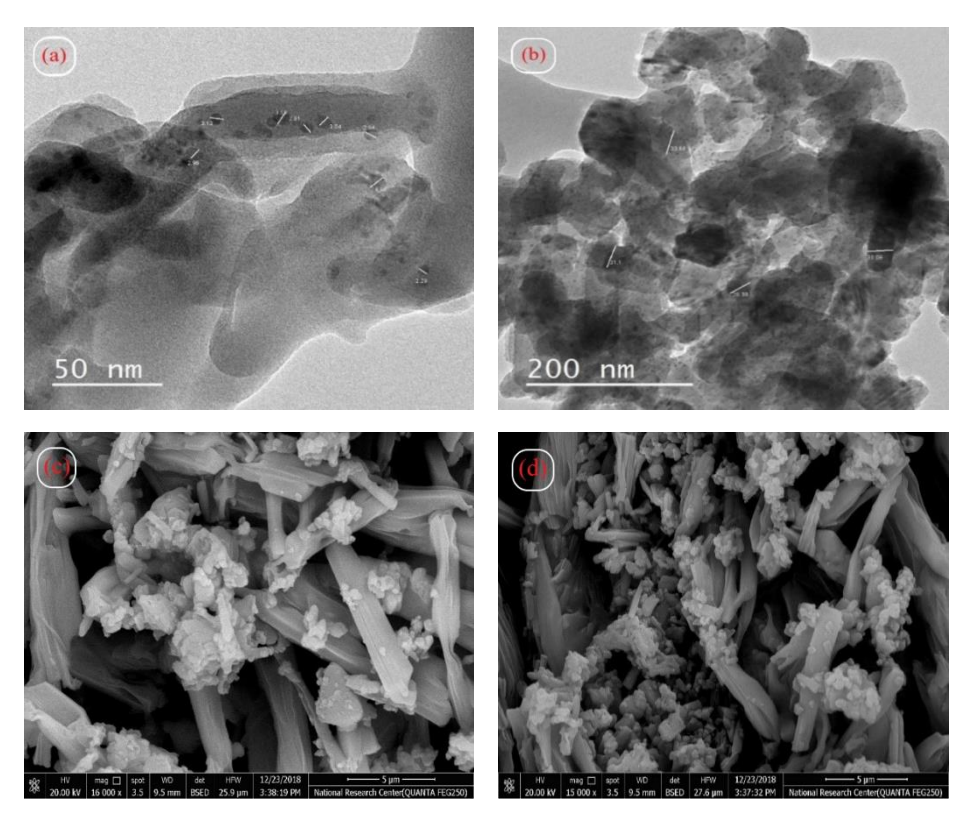


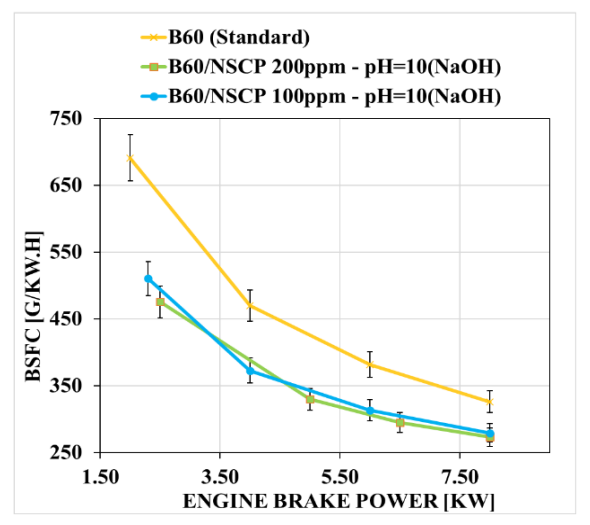
**Figure 3.** (a and b) TEM and (c and d) SEM images of **NTSCP** showing the nanoparticles and the cavity sizes.

## 3.2 Engine attributes at different operating conditions

This study investigation comprises comprehensive measurements of brake-specific fuel consumption (BSFC), braking thermal efficiency (BTE), and exhaust gas temperatures ( $T_{exh}$ ). The  $T_{exh}$  parameter was measured at the exhaust manifold outlet, offering insights into engine combustion characteristics. Experimental analysis has been used to investigate the impacts of **NTSCP** concentration, fuel mixture, and engine load on performance data like BTE, BSFC, and  $T_{exh}$ . The weighted average value for three trials was computed for each experiment. Weighted averages are used to offer an overview of the overall impact of different fuel mixes and engine loads on the measured parameters.

The addition of **NTSCP** shows an evident reduction of BSFC, particularly with the 200-ppm, figure 4. BSFC has been decreased when the concentration of **NTSCP** was 100 ppm but the rate of decrease was not as pronounced as observed with 200 ppm figure 4. Figure 5 represents the outcomes observed for the engine BTE while altering the nanomaterial concentrations in the tested fuel blends. The engine BTE was interestingly enhanced when nanofluids were mixed with B60. The most optimal engine

efficiency value was clearly expressed when 200 ppm of NTSCP was mixed with B60, figure 5. T<sub>exh</sub> results are presented in figure 6. The temperature of the exhaust gases increased with the addition of nanofluids, 100 and 200 ppm concentrations. Moreover, a substantial increase was observed with a 200 ppm concentration of NTSCP. The incorporation of NTSCP increases the surface area for combustion reactions; a significant effect on the combustion process and exhaust gas temperature can be seen. NTSCP stimulates heat transmission and the breakdown of fuel molecules, which leads to better combustion and greater temperatures in the combustion chamber. NTSCP reduces ignition delay and promotes uniform mixing of fuel and air, thus contributing to more consistent and controlled combustion.



B60 (Standard)
B60/NSCP 200ppm - pH=10(NaOH)
B60/NSCP 100ppm - pH=10(NaOH)

35.0

20.0

20.0

15.0

10.0

5.0

0.0

2 4 6 8

ENGINE BRAKE POWER [KW]

**Figure 4.** Measured data of BSFC for different **NTSCP** concentrations.

**Figure 5.** Measured data of BTE for different NTSCP concentrations.

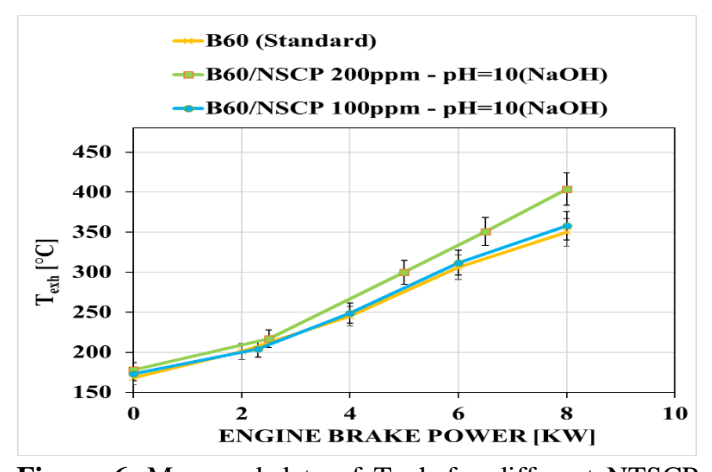


**Figure 6.** Measured data of Texh for different NTSCP concentrations.

# 3.3 Engine exhaust emissions at different operating conditions.

NTSCP catalyses the oxidation reactions of pollutants. These reactions convert hazardous pollutants, such as NO<sub>x</sub>, CO, and volatile organic compounds (VOCs), into less harmful or inert substances. This helps in reducing the overall emission of these pollutants in the exhaust gases [15]. Results of CO emissions presented in figure 7 point out that, the highest levels of CO emissions were recorded for B60 across all engine loads. When B60 was mixed with 100 and 200 ppm of NTSCP, the CO emission levels were lower compared to B60. A substantial decrease was observed with a 200 ppm concentration of NTSCP. CO emissions tend to decrease with increased engine load for all tested fuels. This owing to

the enhanced temperature of combustion during higher load circumstances, resulting in full consumption of carbon, as represented in figure 7.

The CO<sub>2</sub> emission levels were analysed during different engine loads for various fuel feeds including B60, B60 + 100 ppm NTSCP, and B60 + 200 ppm NTSCP. The data in figure 8 indicates that using NTSCP exhibited an average increase in CO<sub>2</sub> emissions values compared to the B60 blend. The maximum CO<sub>2</sub> emission value was observed at B60 + 100 ppm NTSCP, figure 8. The nano-additives are recommended for improving the chemical and physical properties of the fuel mixtures, such as flash points and other combustion-related parameters. When NTSCP is added to the fuel blend the reactivity increases, which might lead to increased CO<sub>2</sub> emissions. As a result of the enhanced thermal conductivity of the fuel mixture including NTSCP, mass and heat transmission increased.

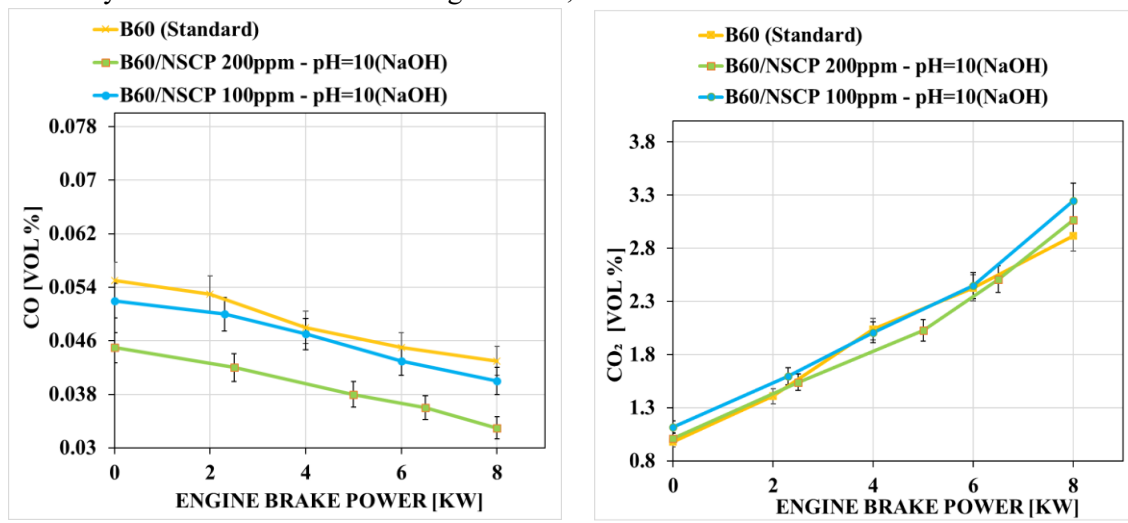
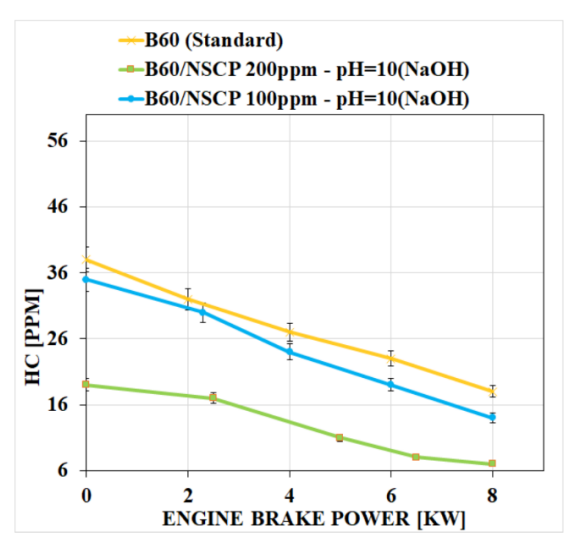


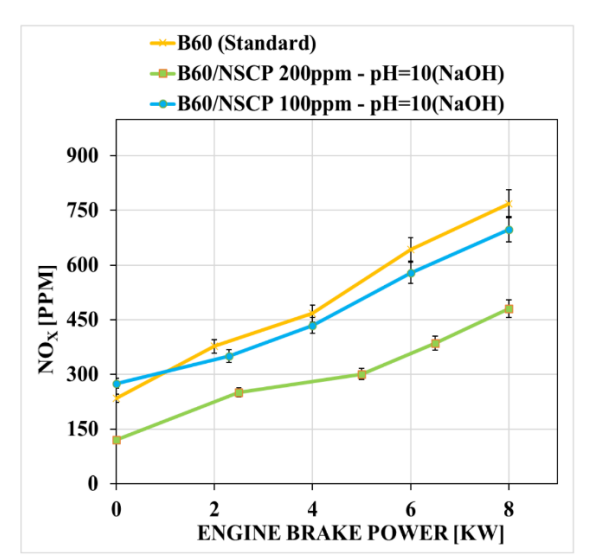
**Figure 7.** Measured data of CO emissions for different **NTSCP** concentrations.

**Figure 8.** Measured data of CO2 emissions for different NTSCP concentrations.

UHC emission levels were examined for different engine loads and fuel feeds, including B60, B60 + 100 ppm NTSCP, and B60 + 200 ppm NTSCP, represented in figure 9. UHC emission levels were observed to be decreased with increasing engine load. This is attributed to a higher combustion temperature. B60 fuel produced the utmost UHC emissions across the whole engine load range, figure 9. When B60 fuel was mixed with different concentrations of NTSCP, the UHC emission levels were reduced. The lowermost UHC emissions were recorded for B60 + 200 ppm NTSCP, figure 9. The oxygen quantity enhances the combustion process, resulting in better combustion and lower UHC emissions. Furthermore, the fuel's properties such as fragmentation and viscosity, possibly be improved by the addition of NTSCP. This results in higher combustion efficiency and lower UHC emissions.

 $NO_x$  emissions, shown in figure 10, were examined for various engine loads and fuel feed including B60, B60 + 100 ppm NTSCP and B60 + 200 ppm NTSCP. B60 exhibited the highest  $NO_x$  emissions over the full engine load range. Data show that adding NTSCP to fuel blends resulted in lower  $NO_x$  emissions compared to B60. In contrast, the lowest  $NO_x$  emissions were measured with B60 + 200 ppm NTSCP, figure 10.  $NO_x$  emissions are known to be impacted by a variety of parameters, like oxygen concentrations, higher combustion temperature, and combustion time. The incorporation of NTSCP in fuel blends reduces  $NO_x$  emissions by significantly shortening engine combustion time. Also, it may have modified the combustion properties, resulting in swift consumption and thus reduced  $NO_x$  emissions.

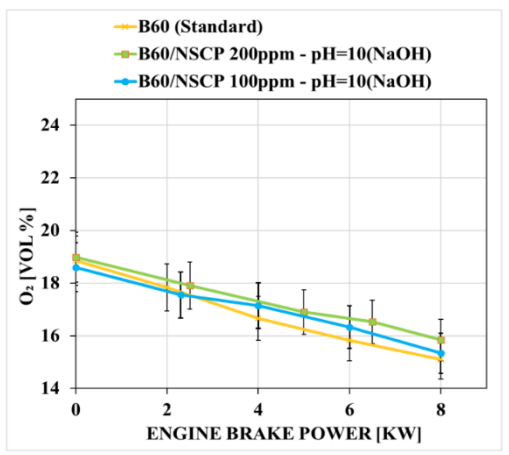




**Figure 9.** Measured data of UHC emissions for different **NTSCP** concentrations.

**Figure 10.** Measured data of NOx emissions for different NTSCP concentrations.

The  $O_2$  emission levels across varying engine loads and the influence of different NTSCP concentrations on these emissions are represented in figure 11. The figure illustrates that  $O_2$  emission levels decrease with an increase in engine load. This is attributed to adequate combustion caused by a greater combustion temperature at higher loads. B60 fuel produced the lowermost  $O_2$  emissions across the whole engine load range, figure 11. When B60 fuel is mixed with different concentrations of NTSCP,  $O_2$  emissions continue to rise. The highest  $O_2$  emissions were recorded for B60 + 200 ppm NTSCP, figure 11. The presence and concentration of NTSCP additions affect the weighted average value of  $O_2$  emissions. It is also noticed that the  $O_2$  emissions value is inversely proportional to the average value of released  $NO_x$ . Lower  $O_2$  emission levels can be due to depletion during the oxidation process and the generation of  $NO_x$ . The data reveal that engine soot production vies with the fast evolution of  $NO_x$  since they both require the CH species, figure 12. It has been noticed that when engine load increases, soot emissions increase. This is related to inadequate combustion caused by a shorter combustion time at high engine loads. B60 fuel produced the utmost soot emissions across the whole engine load range, figure 12. While, when B60 fuel is mixed with different concentrations of NTSCP, soot emissions decrease.



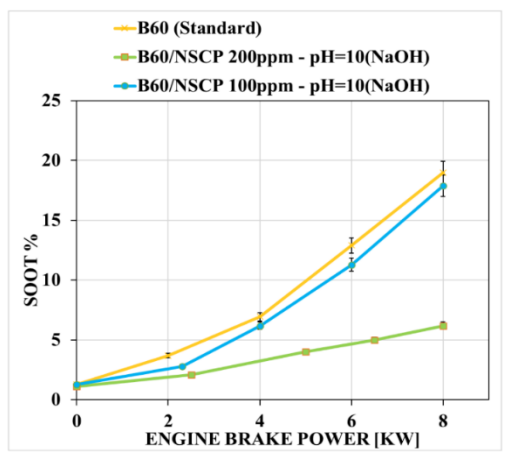


**Figure 11.** Measured data of O2 emissions for different NTSCP concentrations.

**Figure 12.** Measured data of soot emissions for different NTSCP concentrations.

In addition, the lowest soot emissions were measured with B60 + 200 ppm NTSCP, figure 12. The reduction in soot can be attributed to enhanced combustion efficiency, a shorter duration of soot formation, elevated  $O_2$  levels, and possibly influences of ambient temperature on soot generation.

## 5. Conclusion

The findings of this study highlight the significant impact of NTSCP nanomaterial additives on diesel engine performance, particularly in optimizing fuel consumption, enhancing thermal efficiency, and influencing exhaust gas temperatures. Also, the study underscores the significant role of NTSCP nanoadditives in reducing harmful emissions in diesel engines. The experimental results demonstrate that incorporating NTSCP at 100 ppm and 200 ppm concentrations effectively improves combustion characteristics by reducing specific fuel consumption and increasing brake thermal efficiency. Additionally, the rise in exhaust gas temperatures with higher nanomaterial concentrations underscores the role of nano-additives in promoting more complete combustion. The experimental findings confirm that incorporating NTSCP into B60 fuel blends effectively lowers CO, UHC, NO<sub>x</sub>, and soot emissions while increasing CO<sub>2</sub> emissions due to enhanced combustion. Furthermore, the reduction in NO<sub>x</sub> emissions can be attributed to the change in combustion characteristics, which shorten combustion duration and optimize the oxygen-fuel ratio. The observed decrease in soot opacity further demonstrates the ability of NTSCP to enhance fuel-air mixing and combustion kinetics. Overall, the addition of NTSCP at optimized concentrations presents a promising approach for reducing engine emissions while improving combustion performance. Future research should explore long-term engine durability, nanoparticle dispersion stability, and the environmental impact of widespread NTSCP application in real-world conditions.

#### References

- [1] Ye H Y. 2024. The Transformation of Biomass to Bio-nature Gas, Principles and Future Development Trends. *Highlights in Science, Engineering and Technology.* **83**. pp.790-5.
- [2] Guterres A. 2020. The sustainable development goals report. *United Nations publication issued by the Department of Economic and Social Affairs*. pp.1-64.
- [3] Juneja P. 2024. Biomass Waste Conversion Technologies for its Utilization and Energy Generation in India: A Perspective. In *IOP Conference Series: Earth and Environmental Science*. **1285**. p.012010.
- [4] Lević J, Pržulj N and Mandić D. 2023. Biomass as a renewable energy source. *ОДРЖИВИ РАЗВОЈ И УПРАВЉАЊЕ ПРИРОДНИМ РЕСУРСИМА РЕПУБЛИКЕ СРПСКЕ*. **6** (6).
- [5] Nadhir D, Abdelkrim D, Benaoumeur A, Abdellatif O, Sidamar L. 2024. Biofuel Production from Cooking Oil and its Physicochemical Properties. *Studies in Engineering and Exact Sciences*. **5**. pp. e6923-e6923.
- [6] Asase R V, Okechukwu Q N, Ivantsova M N. 2024. Biofuels: present and future. *Environment, Development and Sustainability*. pp.1-29.
- [7] Zheng F and Cho H M. 2024. The comprehensive effects of nano additives on biodiesel-A review. *Energies.* **17** p.4126.
- [8] Kainat S, Gull N, Khan S M, Zia S and Munir S. 2024. Physicochemical attributes, structural characterization, and catalytic properties of nanomaterials. *In Nanomaterials in Biomass Conversion*. pp.143-67.
- [9] Reibold M, Paufler P, Levin A A, Kochmann W, Pätzke N and Meyer D. 2006. Carbon nanotubes in an ancient Damascus sabre. *Nature*. **444**. pp.286-286.
- [10] Gupta A, Kumar R, Maurya A, Ahmadi M H, Ongar B, Yegzekova A, Sharma J P, Kanchan S, Shelare S. 2024. A comparative study of the impact on combustion and emission characteristics

- of nanoparticle-based fuel additives in the internal combustion engine. *Energy Science & Engineering*. **12**. pp.284-303.
- [11] Elkelawy M, Etaiw S E-d H, Bastawissi H A-E, Marie H, Elbanna A, Panchal H, Sadasivuni K and Bhargav H. 2020. Study of diesel-biodiesel blends combustion and emission characteristics in a CI engine by adding nanoparticles of Mn (II) supramolecular complex. *Atmospheric Pollution Research.* 11. pp.117-28.
- [12] Etaiw S E d H, Marie H, Shalaby E M, Farag R S and Elsharqawy F A. 2019. Sensing and photocatalytic properties of nanosized Cu (I) CN organotin supramolecular coordination polymer based on pyrazine. *Applied Organometallic Chemistry*. **33**. p.e5114.
- [13] Scherbaum F, Grohmann A, Müller G and Schmidbaur H. 1989. Synthesis, structure, and bonding of the cation [{(C<sub>6</sub>H<sub>5</sub>) <sub>3</sub>PAu} <sub>5</sub>C]<sup>⊕</sup>. *Angewandte Chemie International Edition in English.* **28**. pp.463-5.
- [14] Steigelmann O, Bissinger P and Schmidbaur H. 1990. Assembly of the [CAu<sub>6</sub>] <sup>2</sup> Cluster with a Tailor-made Diphosphane Spanning the Octahedral Edges. *Angewandte Chemie International Edition in English.* **29**. pp.1399-400.
- [15] Tomatis M, Xu H-H, He J and Zhang X-D. 2016. Recent development of catalysts for removal of volatile organic compounds in flue gas by combustion: a review. *Journal of Chemistry*. (1) p.8324826.